



Published in final edited form as:

Neuroimage. 2024 January ; 285: 120502. doi:10.1016/j.neuroimage.2023.120502.

Distance from main arteries influences microstructural and functional brain tissue characteristics

**Viktor Weiss^{a,b}, Viktória Kokošová^{a,c}, Zdeněk Valenta^d, Irena Doležalová^a, Marek Baláž^a,
Silvia Mangia^e, Shalom Michaeli^e, Lubomír Vojtíšek^f, Igor Nestrašil^e, Roman Herzig^{b,g},
Pavel Filip^{e,h,*}**

^aFirst Department of Neurology, Faculty of Medicine, Masaryk University and University Hospital of St. Anne, Brno, Czech Republic

^bDepartment of Neurology, Charles University Faculty of Medicine, Hradec Králové, Czech Republic

^cDepartment of Neurology, Faculty of Medicine, Masaryk University and University Hospital Brno, Brno, Czech Republic

^dDepartment of Statistical Modelling, Institute of Computer Science of the Czech Academy of Sciences, Prague, Czech Republic

^eCenter for Magnetic Resonance Research (CMRR), University of Minnesota, Minneapolis, MN, United States of America

^fCentral European Institute of Technology (CEITEC) Masaryk University, Neuroscience Centre, Brno, Czech Republic

^gDepartment of Neurology, Comprehensive Stroke Center, University Hospital Hradec Králové, Czech Republic

^hDepartment of Neurology, Charles University, First Faculty of Medicine and General University Hospital, Prague, Czech Republic

Abstract

Given the substantial dependence of neurons on continuous supply of energy, the distribution of major cerebral arteries opens a question whether the distance from the main supply arteries constitutes a modulating factor for the microstructural and functional properties of brain tissue. To tackle this question, multimodal MRI acquisitions of 102 healthy volunteers over the full

This is an open access article under the CC BY-NC-ND license (<http://creativecommons.org/licenses/by-nc-nd/4.0/>).

*Corresponding author at: Postal address: Neurologická klinika 1. LF a VFN, Kateřinská 468, Prague 120 00, Czech Republic. pvlfilip@gmail.com (P. Filip).

CRedit authorship contribution statement

Viktor Weiss: Conceptualization, Writing – original draft. **Viktória Kokošová:** Validation, Writing – review & editing, Visualization. **Zdeněk Valenta:** Methodology, Writing – review & editing. **Irena Doležalová:** Conceptualization, Writing – original draft. **Marek Baláž:** Visualization, Writing – review & editing. **Silvia Mangia:** Conceptualization, Writing – review & editing. **Shalom Michaeli:** Conceptualization, Writing – review & editing. **Lubomír Vojtíšek:** Data curation, Funding acquisition, Writing – review & editing. **Igor Nestrašil:** Writing – review & editing. **Roman Herzig:** Writing – review & editing. **Pavel Filip:** Conceptualization, Funding acquisition, Formal analysis, Writing – original draft.

Declaration of Competing Interest

There are no potential conflicts of interests and no financial relationships regarding this paper which could bias this work.

adult age span were utilised. Relaxation along a fictitious field in the rotating frame of rank $n = 4$ (RAFF4), adiabatic T1 ρ , T2 ρ , and intracellular volume fraction (fICVF) derived from diffusion-weighted imaging were implemented to quantify microstructural (cellularity, myelin density, iron concentration) tissue characteristics and degree centrality and fractional amplitude of low-frequency fluctuations to probe for functional metrics. Inverse correlation of arterial distance with robust homogeneity was detected for T1 ρ , T2 ρ and RAFF4 for cortical grey matter and white matter, showing substantial complex microstructural differences between brain tissue close and farther from main arterial trunks. Albeit with wider variability, functional metrics pointed to increased connectivity and neuronal activity in areas farther from main arteries. Surprisingly, multiple of these microstructural and functional distance-based gradients diminished with higher age, pointing to uniformization of brain tissue with ageing. All in all, this pilot study provides a novel insight on brain regionalisation based on artery distance, which merits further investigation to validate its biological underpinnings.

Keywords

Quantitative MRI; Relaxometry; Diffusion weighted imaging; Resting-state functional MRI; Arterial distance

1. Introduction

The human brain is responsible for about 20 % of our total energy expenditure, although accounting only for 2 % of the body weight (Attwell and Laughlin, 2001). It is not only nutrients, but also oxygen, that need to be supplied to its every part. Its vasculature is an essential component of the structure, both in the cortex and subcortical areas. There are macroscopic vessels mostly running over the pial surface, branching into diving arteries at the mesoscopic scale penetrating into deeper structures, and ultimately into dense networks of capillaries (Schmid et al., 2019). Furthermore, vascular density definitely varies all over the brain, not only with the obvious distance from the main major cerebral arteries, but also with cortical depth (Duvernoy et al., 1981). Moreover, the brain is capable to regulate cerebral blood flow (Chen et al., 2014; Hawkins and Davis, 2005) via cerebral blood flow and metabolism coupling to reflect its metabolic needs. Both extremes, hypoperfusion, and hyperperfusion are unwanted phenomena with tangible clinical signatures. Hypoperfusion causes brain ischaemia ultimately leading to ischaemic stroke, while brain hyperperfusion may lead to cerebral hyperaemia, increased brain pressure, and subsequent neuronal damage (Venkat et al., 2016).

The distribution of major arteries on the cortical surface opens a question whether nutrient and oxygen supply in areas more distant is as effective as in their proximity. Possible tissue vulnerabilities in areas that are more distant from major arteries may be reflected by subtle alterations in microstructural and functional properties. Under pathologically low blood flow conditions, we often witness a possible clinical correlate of this hypothesis, namely watershed strokes, i.e. areas of brain ischaemia localised in vulnerable border zones between major arteries (Selvanayaki and Sasikala, 2020). Furthermore, brain aging may further accentuate tissue alterations in areas more distant from the main arteries, since

aging is associated with not only vascular system deterioration, but also with neurovascular uncoupling, i.e., the disruption between brain metabolism requirements and blood supply (Agarwal et al., 2016; Østergaard et al., 2014).

Assessing whether the distance from the main supply arteries constitutes a modulating factor for the microstructural and functional properties of brain tissue requires a modality able to extract information about microstructure and potentially also functional characteristics in vivo. Magnetic resonance imaging (MRI), with its ability to tune protocols to various tissue characteristics, provides such an opportunity. The fundamental concept of MRI is the utilisation of water molecules as sensitive probes of local microenvironment. While true microstructural elements as neurons, their dendrites and axons cannot be directly visualised utilising in vivo MRI, some global information about tissue microstructure is retained. Even though blurred and indirect, it allows for inferences about myelination (Stüber et al., 2014), presence of iron (Möller et al., 2019), cellularity, neuronal fibre distribution (Palombo et al., 2020) and function (Ekstrom, 2010).

Hence, this pilot study was designed to utilise multimodal MRI acquisition protocol with the intent to extract quantitative MRI (qMRI) parameters describing various biological features and ascertain their dependence on the distance from the closest major artery. Various aspects of brain microstructure were described using the following parameters: cellular density via adiabatic rotating frame longitudinal relaxation time constant – $T1\rho$ (Michaeli et al., 2009), iron level via adiabatic rotating frame transverse relaxation time constant – $T2\rho$ (Michaeli et al., 2005; Mitsumori et al., 2009), myelin density via non-adiabatic Relaxation Along a Fictitious Field in the rotating frame of rank 4 (RAFF4) (Hakkarainen et al., 2016; Liimatainen et al., 2015; Satzer et al., 2015) and intracellular volume fraction (fICVF) as a parameter derived from diffusion-weighted imaging (DWI) (Tariq et al., 2016). Furthermore, two functional resting-state MRI metrics were considered: weighted Degree Centrality (wDeCe) describing global connectivity and fractional amplitude of low-frequency fluctuations (fALFF) as a measure of spontaneous neural activity of the brain (Zang et al., 2007). The study focused on answering three main questions:

1. Whether the distance from main arterial blood supply sources (hereinafter AD – arterial distance) in the brain is mirrored in relevant qMRI microstructural and/or functional parameters – a parameter labelled as AD-qMRI correlation (arterial distance – quantitative MRI metric correlation);
2. Whether ageing affects brain microstructure and/or function differently based on the distance from the closest main artery;
3. Whether general fitness level impacts eventual alterations associated with arterial distance and age.

We hypothesised that AD is a major factor defining regionality of microstructural and functional parameters, as we speculated that areas that are more distant would suffer by more limited access to oxygen and nutrients as compared to brain areas closer to main arteries. Furthermore, we expected that higher age accentuated these differences, which would be countered by general health and fitness.

2. Methods

2.1. Subjects

116 healthy, non-demented volunteers underwent the screening procedures for this study. This population is shared with a previously published study on ageing (Filip et al., 2023). The collected data included basic demographic information, body height and weight to calculate body mass index (BMI), International Physical Activity Questionnaire, the short self-administered version (IPAQ-SF) (Lee et al., 2011), and the Brief Questionnaire Regarding Severity of Memory & Emotional Problems (BQRS-M&E) (Reisberg, 2013) – a screening, patient-facing 5-item subjective scale on eventual cognitive problems. The following exclusion criteria were implemented: general MRI contraindications, claustrophobia, the presence of a substantial space occupying or vascular lesion in the MRI scan, subcortical leukoencephalopathy exceeding Fazekas stage I, psychiatric and/or neurologic disorder, subjectively perceived cognitive problems (BQRS-M&E ≥ 3). Every participant gave a written informed consent in accordance with the Declaration of Helsinki. The study protocol was approved by the Ethics Committee of the University Hospital of St. Anne, Czech Republic (approval code 38V/2018).

2.2. Imaging protocol and data analysis

MRI scans were acquired using a 3-Tesla Siemens MAGNETOM Prisma scanner at the Central European Institute of Technology (CEITEC) in Brno, Czech Republic, using a previously published MRI protocol (Filip et al., 2020a), consisting of T1-weighted (T1w), T2-weighted (T2w), adiabatic T1 ρ , T2 ρ and non-adiabatic RAFF4, DWI and rs-fMRI acquisition. Briefly, the following parameters were utilised:

- T1w: magnetization-prepared rapid gradient echo (MPRAGE), 1.0 mm isotropic resolution, repetition time (TR) 2150 ms, echo time (TE) 2.47 ms, inversion time (TI) 1100 ms, flip angle (FA) 8°, generalized autocalibrating partial parallel acquisition (GRAPPA) of 2.
- T2w: SPACE sequence, 1.0 mm isotropic resolution, TR 2820 ms, TE 72.6 ms, GRAPPA 2.
- Rotating frame relaxation measurements (adiabatic T1 ρ , T2 ρ and non-adiabatic RAFF4): voxel size of 1.6 \times 1.6 \times 3.6 mm (Duvernoy et al., 1981) in 30 slices, GRAPPA 3, TR = 2000 ms, TE 3.18 ms (for more information see (Filip et al., 2020a)).
- DWI: 1.8 mm isotropic resolution, TR 2820 ms, TE 72.6 ms, MB 4, 93 directions with 7 additional non-diffusion weighted (b0) images, b-shells of 750 and 1500 s/mm (Schmid et al., 2019); two separate acquisitions with opposite phase encoding polarity (anterior-posterior (AP) followed by posterior-anterior (PA)).
- rs-fMRI: gradient-recalled echo (GRE) echo-planar imaging (EPI) sequence, 3.0 mm isotropic resolution, TR 900 ms, TE 30.0 ms, FA 45°, MB 4, interleaved acquisition, consisting of 502 vol.

The processing of T1w and T2w scans, rsf-MRI and DWI was based on the Human Connectome Project (HCP) minimal pre-processing pipeline (Glasser et al., 2013), followed by HCP rs-fMRI pipeline (Smith et al., 2013). DWI post-processing extracted the NODDI parameter of interest – fICV (Tariq et al., 2016). AFNI package (Cox, 1996) was used to calculate voxel-wise weighted degree centrality (DeCe) with sparsity threshold of 0.1 and fALFF for the frequency range of 0.01 to 0.1 Hz (Zang et al., 2007) from rs-fMRI data. The processing pipeline for rotating frame relaxation acquisitions included motion correction, the calculation of the relaxation time constant with 2-parameter non-linear fitting for T1 ρ and T2 ρ , and 4-parameter non-linear fitting for RAFF4, and 3D rigid body co-registration to the T1w scan. ROI masks were derived from the automatic FreeSurfer segmentation (cerebral cortical GM; subcortical GM and whole WM) and co-registered to the images with lower resolution to avoid oversampling.

For each voxel in the MNI space, the distance to the nearest artery was calculated as its Euclidean distance to the nearest artery in the binarized Statistical Atlas of Cerebral Arteries (Mouches and Forkert, 2019). Afterwards, cortical GM voxels were mapped to the 2-mm standard Connectivity Informatics Technology Initiative (CIFTI) grayordinate space utilising partial volume weighted ribbon-constrained volume to surface mapping algorithm to create the cortical surface reconstruction (see Fig. 1).

Quality control of all data processing outputs, including motion, was performed by two trained operators (V.K. and P.F.).

In addition to the basic summary of demographic information and data on general fitness (BMI, IPAQ-SF – presented in the format MET-min per day), Spearman's correlation coefficients were calculated between age, BMI and IPAQ-SF, after correcting for the effect of sex. In the statistical analysis of the Aim 1, AD-qMRI correlation was calculated as voxel-wise Spearman's rank correlation coefficient of individual MRI metrics of interest (subject-specific T1 ρ , T2 ρ , RAFF4, fICVF, wDeCe, fALFF in GM ROIs and T1 ρ , T2 ρ , RAFF4, fICVF in the WM ROI) with the above-described artery distance map (common for all subjects) over preselected ROIs (cortical GM, subcortical GM, WM) for each subject. Ergo, for each subject, this approach provided one correlation coefficient for every ROI-MRI metric combination (16 CE-qMRI correlation coefficients per subject in total). Two-tailed one-sample *t*-test was used to assess whether subject-specific Fisher transformed AD-qMRI correlation over predetermined ROIs were statistically significantly different from zero (Aim 1). The Aim 2 was evaluated based on Pearson's correlation coefficient of subject-specific Fisher transformed AD-qMRI correlation and age. Lastly, for the Aim 3, four GLMs were used. The above-described subject-specific Fisher transformed AD-qMRI correlations were considered dependent variables and sex a covariate of non-interest in all of them. In the analysis of the primary effect of BMI and IPAQ-SF, BMI and IPAQ-SF were considered independent variables and age was utilised as another covariate of non-interest (two separate GLMs). In the analysis of the interaction of age and general fitness, age and BMI in the third GLM, and age and IPAQ-SF in the fourth GLM were considered independent variables, whose interaction was of interest for the statistical output. False discovery rate (FDR) correction was implemented over MRI metrics (6 in GM, 4 in WM) and ROIs (3) for all the aims separately, with alpha of 0.05 as the type I error threshold.

3. Results

From the 116 recruited subjects, 7 were excluded due to incomplete acquisition and/or excessive motion. In addition, BQRS-M&E, IPAQ-SF and/or demographic data was lost in 3 subjects and further 4 subjects were excluded due to the presence of subjective cognitive problems based on BQRS-M&E score, leaving in total 102 subjects for the analysis (see Table 1 for the overview of basic information). Other than the correlation between Age and BMI ($\rho = 0.283$, $p_{\text{FDR-cor}} = 0.013$), there was no statistically significant association between the age, general activity levels and BMI.

Aim 1: Effect of distance from arterial supply on qMRI metrics –

As seen in the Table 2, all the AD-qMRI correlation values were statistically significantly different from 0, with extremely low p values and large effect sizes. Fig. 2 provides an overview showing that in both GM ROIs, microstructural metrics (T1 ρ , T2 ρ , RAFF4, fICVF) exhibited generally negative correlations with AD, while AD-qMRI correlation for fMRI metrics were in the positive range. In the WM, T1 ρ , T2 ρ and RAFF4 were anticorrelated with AD, while fICVF showed positive correlation. Furthermore, even though the absolute values of correlation coefficients were rather low, they were highly consistent over all microstructural metrics, as evident in the high clustering of individual datapoints in the Fig. 2 and very high effect sizes (see Table 2). Even fMRI metrics yielded a reasonable clustering, with effect size still in the large range (>0.8).

Aim 2: Effect of age on AD-qMRI correlation values –

Table 2 and Fig. 2-A show for cortical GM a statistically significant effect of age on AD-qMRI of RAFF4 and fICVF, with an age-associated increase in the AD-RAFF4 correlation, but still in negative ranges, and age-associated decrease of AD-fICVF correlation, going from mildly positive values to negative range. In WM (Fig. 2-B), only AD-fICVF correlation was significantly correlated with age, again with lower parameter values in higher age groups, still in the positive correlation range. In the subcortical GM, age was associated with the drop of AD-RAFF4, AD-wDeCe and AD-fALFF correlation from positive range towards zero (Fig. 2-C).

Aim 3: Effect of general fitness and its interaction with age on AD-qMRI correlation values –

All GLMs failed to detect any statistically significant interactions.

4. Discussion

To our knowledge, this is the first study to analyse the relationship between the distance to the closest main artery and qMRI metrics as proxies of microstructural and functional characteristics. While the relationship between blood flow and neuronal function or the very ability of neurons to survive has seen its well-earned attention in the research of stroke, ischaemic penumbra and its clinical implications (Ermine et al., 2021), the question of whether tissue characteristics are associated with distance from main arteries also in non-pathological states has largely eluded the focus of neuroscientists. Nonetheless, our results

clearly show that even far smaller micro-environment differences related to the arterial support than the extreme seen in stroke are mirrored in multiple tissue characteristics.

One of the major aspects of the presented study is the utilised estimation of Euclidean distances to the nearest artery. While it is tempting to see this metric as a direct proxy of regional blood flow, this oversimplification neglects the ability of the brain to dynamically adjust energy supply from the vascular system to meet the local demands, and also the differences in the terminal capillary network in individual areas. Moreover, different areas of brain tend to use energy at different rates even at rest (Karbowski, 2011) and newer views propose the supply as the constraining factor for the regional rates of energy use (Herculano-Houzel and Rothman, 2022), further complicating the issue. Nonetheless, local cerebral blood flow measured utilising arterial spin labelling has been previously associated with alterations of diffusion tensor metrics in WM (Giezendanner et al., 2016; Chen et al., 2013). Although these parameters provide only a simplistic view on the underlying tissue avoiding more intricate characteristics of WM (Tournier et al., 2011), our findings of a negative correlation of all the relaxation metrics with AD in both cortical GM and WM generally corroborate these reports. Furthermore, more complex models of myelin water fraction pointed to myelin content decline with cerebral blood flow (Bouhrara et al., 2022).

The relaxation metrics presented in this study exhibited an inverse correlation with AD in cortical GM and WM, with high degree of homogeneity as evident in the tight clustering of individual datapoints in the Fig. 2. However, it would be unwise to see these metrics as direct proxies of any specific tissue characteristics under the circumstances considered in this study. Previous body of research has found $T1\rho$, adiabatic rotating frame longitudinal relaxation time, to be inversely related to cellular loss and partly myelination (Michaeli et al., 2007, 2009). Furthermore, this metric exhibits very high sensitivity to alterations present in demyelination diseases (Filip et al., 2020a, 2021), where it was able to detect alterations even in normally appearing WM, neurodegeneration (Filip et al., 2020b; Tuite et al., 2012) and also ageing (Filip et al., 2023). $T2\rho$, adiabatic rotating frame transverse relaxation time, exhibits inverse correlation with arterial distance in all the considered ROIs. It has been previously associated with iron concentration (Michaeli et al., 2005; Mitsumori et al., 2009), corroborated in clinical settings as a metric highly sensitive to cortical alterations in primary progressive sclerosis (Filip et al., 2021) but also in ageing (Filip et al., 2023). Lastly, RAFF4, a metric previously associated with myelin content (Hakkarainen et al., 2016; Liimatainen et al., 2015; Satzer et al., 2015; Holikova et al., 2021), with high sensitivity in demyelination diseases and expectable U-shaped curve in ageing (Filip et al., 2023), showed inverse correlation in cortical GM and WM, but direct correlation in subcortical GM.

Nonetheless, since all these metrics are generally sensitive to multiple microstructural characteristics, with supposed dominance of certain components, inferences on the histological nature of the reported changes are rather speculative. However, the same is true for virtually any available quantitative MRI metric. For instance, the ratio of T1-weighted and T2-weighted signal labelled “myelin map” based on the similarity to cytoarchitectonic maps has been repeatedly challenged due to generally low support with extensive histological studies especially in the presence of pathology (Uddin et al., 2018; Desmond et al., 2016). Even complex metrics are not devoid of doubt, e.g. myelin water

fraction, previously repeatedly published as a marker exquisitely sensitive to myelin, is still significantly affected by iron present in the tissue (Birkl et al., 2019). Moreover, myelin-related qMRI parameters are exceedingly difficult to interpret in wide age-span cohorts due to their inability to distinguish between fully functional and redundant myelin affected by ballooning, splits and further age-related alterations. This characteristic is of paramount importance for the function of the tissue (Peters, 2002). In the light of previously published histological validation studies and studies in relevant disease models, our findings point to significant association of AD with myelin density, iron and cellularity in all the brain tissue types. Multimodal studies including histological validations under identical pathophysiological circumstances will be of uttermost importance to shed light on the true nature of AD-related alterations, with possible implications in both chronic cerebrovascular diseases as subcortical leukoencephalopathy or acute conditions as watershed strokes. These microstructural differences between tissues close to the main arteries and tissues farther away may present a hidden vulnerability warranting research in relevant patient groups. fMRI measures yielded positive correlations with arterial distance in all the GM regions. Ergo, GM areas farther from the main arteries are more interconnected with the rest of the brain and exhibit larger low-frequency activity than regions in close proximity to main arteries. Moreover, no age-related changes to this regionality were detected in the cortical GM. Though, one must consider the distribution of the cortical arterial distance map (Fig. 1-A), where multiple areas generally seen with higher global functional connectivity supposedly due to the nature of their function (Zuo et al., 2012) are located in regions more distant from the closest main artery.

The analysis of age effect must be considered in the light of the changes of the utilised MRI metrics over the age span, as previously published for this cohort (Filip et al., 2023). All the MRI metrics implemented in the presented paper showed substantial simple association with age. However, in the more nuanced, localised rendering presented here, there were no changes in AD-T1 ρ and AD-T2 ρ correlations in all the ROIs, despite the marked, nearly exponential age-related increase in both these MRI metrics in these ROIs (Filip et al., 2023). AD-qMRI correlation of cortical fMRI parameters also remained unaltered, while the AD-based regionality of both connectivity and low-frequency activity seemed to subside from positive AD-qMRI correlations towards zero (Fig. 3). On the other hand, cortical AD-fICVF correlation departed from values close to zero in young age towards the negative range, i.e. the older the subject was, the smaller was the intracellular volume in areas more distant from the closest main artery. In the subcortical GM areas, higher age was associated with lower AD-related regionality of fMRI parameters, but also myelination (Fig. 3). Hence, these data opposed our initial hypothesis: other than for cortical fICVF-AD correlation, the distance from the artery was a less defining factor for the microstructural and functional characteristics in older people and the tissue became more uniform with age. Whether this finding is related to the previously described higher resilience of phylogenetically older structures (Gebel et al., 1998) remains to be further explored.

Lastly, the analysis with possibly the highest universal and clinical implications is the effect of general fitness as a proxy of the vascular condition on the above-described iron, myelination and cellularity characteristics. However, it failed to produce significant results. The hypothesis seems sound and generally well supported by previous research

(d'Arbeloff, 2020; Kramer et al., 2003). Nonetheless, no effect of general health was found on the AD-qMRI correlations or their ageing-associated changes. We may only speculate on the true causes of this counter-intuitive result, be it the low reliability of subjective retrospective evaluation in IPAQ-SF, as seen in the lack of its correlation with objective measures of activity levels published previously (Lee et al., 2011), oversimplified nature of BMI or general complexity of the implemented statistical model lacking sufficient power to detect relevant changes for this cohort size. Therefore, objective measures of activity (e.g. monitoring of number of steps, long-term body accelerometric data etc.) and more comprehensive examination of general health would definitely be of major benefit for further evaluations of its effect on brain health and AD-related regionality detected in this study.

Several major limitations must be considered when interpreting this study. Although it is not uncommon in the literature to parallel biological underpinnings and qMRI parameters directly, a word of caution is in order. MRI provides information generally highly sensitive to any physiological or pathological alteration, but the specificity of any derived metrics is its main hindrance. Even though histological validation (Mitsumori et al., 2009; Satzer et al., 2015) with confirmation in relevant diseases (Filip et al., 2020a, 2021) is available for multiple presented qMRI metrics, all qMRI values inherently are compounds of various underlying features and under different circumstances, different individual contributors to the signal may become dominant. The same holds true for fICVF in WM and especially GM which, although repeatedly published in relevant pathologies (Kamiya et al., 2020), has been challenged at multiple levels e.g. due to the overestimation of multiple components (Alsameen et al., 2020; Guerrero et al., 2019). Furthermore, the cross-sectional nature of the study hinders further inferences for the aim 2 – evaluation of age effect on AD-qMRI correlation values. Longitudinal designs are far more suitable for ageing research, but suffer from high financial burden, complexity issues and practicality problems in following subjects for timespans sufficient for age-related microstructural changes of interest to develop. Lastly, the acquisition protocol of this study did not implement any pure angiographic sequences and the analysis was based on a well-defined, but still uniformised atlas neglecting certain subject individuality in this matter. Therefore, the study focused only on major arteries exhibiting substantial stability when compared to smaller vessels. Further studies building upon this project and designed to extract more precise information in closer vicinity of arteries should definitely consider the inclusion of angiographic protocols, possibly with the administration of contrast agents to achieve reasonable resolution and precision.

5. Conclusion

All in all, this study provides the first indication of arterial distance as an important element affecting microstructural and functional measures both in GM and WM. The presented multimodal MRI protocol points to significant complex microstructural and functional gradients related to the distance to the closest main artery, encompassing myelin density, cellularity and iron. With higher age, multiple of these findings tended to diminish. This new insight definitely warrants further investigations, possibly even beyond non-invasive MRI acquisitions, and extension to relevant neurovascular pathological conditions.

Acknowledgments

Financial support for this project was provided by the General University Hospital in Prague (MH CZ-DRO-VFN64165) and the Center for Magnetic Resonance Research NIH core grant P41EB027061. We acknowledge the core facility MAFIL of CEITEC supported by the MEYS CR (LM2018129 Czech-BioImaging). P.F., V.W. and R.H. were supported by Charles University, Czech Republic (Cooperatio Program, research area NEUR). R.H. was supported by the Ministry of Health of the Czech Republic (grant No. DRO – UHHK 00179906).

Data availability

Raw or processed data of this study are not publicly available due to the sensitive nature of human data acquired in patients. The data is available upon reasonable request to the corresponding author.

Abbreviations:

AD	arterial distance
MRI	magnetic resonance imaging
rsfMRI	resting-state functional MRI
qMRI	quantitative MRI
T1w	T1-weighted
T2w	T2-weighted
DWI	diffusion-weighted imaging
RAFF4	relaxation along a fictitious field of rank 4
fICVF	intracellular volume fraction
wDeCe	weighted degree centrality
fALFF	fractional amplitude of low-frequency fluctuations
ROI	region of interest
GM	grey matter
WM	white matter

References

- Agarwal S, Sair HI, Yahyavi-Firouz-Abadi N, et al. , 2016. Neurovascular uncoupling in resting state fMRI demonstrated in patients with primary brain gliomas. *J. Magn. Reson. Imaging JMRI* 43, 620–626. [PubMed: 26201672]
- Alsameen MH, Gong Z, Qian W, et al. , 2020. C-NODDI: a constrained NODDI model for axonal density and orientation determinations in cerebral white matter. *Front Neurol* 14.
- Attwell D, Laughlin SB, 2001. An energy budget for signaling in the grey matter of the Brain. *J. Cereb. Blood Flow Metab* 21, 1133–1145. [PubMed: 11598490]
- Birkel C, Birkel-Toeglhofer AM, Endmayr V, et al. , 2019. The influence of brain iron on myelin water imaging. *Neuroimage* 199, 545–552. [PubMed: 31108214]

- Bouhrara M, Triebswetter C, Kiely M, et al. , 2022. Association of cerebral blood flow with longitudinal changes in cerebral microstructural integrity in the Coronary Artery Risk Development in Young Adults (CARDIA) study. *JAMA Netw. Open* 5, e2231189. [PubMed: 36094503]
- Chen JJ, Rosas HD, Salat DH, 2013. The relationship between cortical blood flow and sub-cortical white-matter health across the adult age span. *PLoS One* 8, e56733. [PubMed: 23437228]
- Chen J, Venkat P, Zacharek A, et al. , 2014. Neurorestorative therapy for stroke. *Front. Hum. Neurosci* 8, 382. [PubMed: 25018718]
- Cox RW, 1996. AFNI: software for analysis and visualization of functional magnetic resonance neuroimages. *Comput. Biomed. Res* 29, 162–173. [PubMed: 8812068]
- d'Arbeloff T, 2020. Cardiovascular fitness and structural brain integrity: an update on current evidence. *GeroScience* 42, 1285–1306. [PubMed: 32767221]
- Desmond KL, Al-Ebraheem A, Janik R, et al. , 2016. Differences in iron and manganese concentration may confound the measurement of myelin from R1 and R2 relaxation rates in studies of dysmyelination. *NMR Biomed.* 29, 985–998. [PubMed: 27226282]
- Duvernoy HM, Delon S, Vannson JL, 1981. Cortical blood vessels of the human brain. *Brain Res. Bull* 7, 519–579. [PubMed: 7317796]
- Ekstrom A, 2010. How and when the fMRI BOLD signal relates to underlying neural activity: the danger in dissociation. *Brain Res. Rev* 62, 233–244. [PubMed: 20026191]
- Ermine CM, Bivard A, Parsons MW, et al. , 2021. The ischemic penumbra: from concept to reality. *Int. J. Stroke* 16, 497–509. [PubMed: 33818215]
- Filip P, Svatkova A, Carpenter AF, et al. , 2020a. Rotating frame MRI relaxations as markers of diffuse white matter abnormalities in multiple sclerosis. *NeuroImage Clin.* 26, 102234. [PubMed: 32272373]
- Filip P, Vojtíšek L, Baláž M, et al. , 2020b. Differential diagnosis of tremor syndromes using MRI relaxometry. *Parkinsonism Relat. Disord* 81, 190–193. [PubMed: 33186797]
- Filip P, Dufek M, Mangia S, et al. , 2021. Alterations in sensorimotor and mesiotemporal cortices and diffuse white matter changes in primary progressive multiple sclerosis detected by adiabatic relaxometry. *Front. Neurosci* 1129.
- Filip P, Kokošová V, Valenta Z, et al. , 2023. Utility of quantitative MRI metrics in brain ageing research. *Front. Aging Neurosci* 15, 1099499. [PubMed: 36967815]
- Gebel JM, Sila CA, Sloan MA, et al. , 1998. Thrombolysis-related intracranial hemorrhage. *Stroke* 29, 563–569. [PubMed: 9506593]
- Giezendanner S, Fislser MS, Soravia LM, et al. , 2016. Microstructure and cerebral blood flow within white matter of the human brain: a TBSS analysis. *PLoS One* 11, e0150657. [PubMed: 26942763]
- Glasser MF, Sotiropoulos SN, Wilson JA, et al. , 2013. The minimal preprocessing pipelines for the human connectome project. *Neuroimage* 80, 105–124. [PubMed: 23668970]
- Guerrero JM, Adluru N, Bendlin BB, et al. , 2019. Optimizing the intrinsic parallel diffusivity in NODDI: an extensive empirical evaluation. *PLoS One* 14, e0217118. [PubMed: 31553719]
- Hakkarainen H, Sierra A, Mangia S, et al. , 2016. MRI relaxation in the presence of fictitious fields correlates with myelin content in normal rat brain. *Magn. Reson. Med* 75, 161–168. [PubMed: 25648507]
- Hawkins BT, Davis TP, 2005. The blood-brain barrier/neurovascular unit in health and disease. *Pharmacol. Rev* 57, 173–185. [PubMed: 15914466]
- Herculano-Houzel S, Rothman DL, 2022. From a demand-based to a supply-limited framework of brain metabolism. *Front. Integr. Neurosci* 16, 818685. [PubMed: 35431822]
- Holikova K, Laakso H, Salo R, et al. , 2021. RAFF-4, magnetization transfer and diffusion tensor MRI of lysophosphatidylcholine induced demyelination and remyelination in rats. *Front. Neurosci* 15, 148.
- Kamiya K, Hori M, Aoki S, 2020. NODDI in clinical research. *J. Neurosci. Methods* 346, 108908. [PubMed: 32814118]
- Karbowski J, 2011. Scaling of brain metabolism and blood flow in relation to capillary and neural scaling. *PLoS One* 6, e26709. [PubMed: 22053202]

- Kramer AF, Colcombe SJ, McAuley E, et al. , 2003. Enhancing brain and cognitive function of older adults through fitness training. *J. Mol. Neurosci* 20, 213–221. [PubMed: 14501000]
- Lee PH, Macfarlane DJ, Lam TH, et al. , 2011. Validity of the international physical activity questionnaire short form (IPAQ-SF): a systematic review. *Int. J. Behav. Nutr. Phys. Act* 8, 1–11. [PubMed: 21194492]
- Liimatainen T, Hakkarainen H, Mangia S, et al. , 2015. MRI contrasts in high rank rotating frames. *Magn. Reson. Med* 73, 254–262. [PubMed: 24523028]
- Möller HE, Bossoni L, Connor JR, et al. , 2019. Iron, myelin, and the brain: neuroimaging meets neurobiology. *Trends Neurosci.* 42, 384–401. [PubMed: 31047721]
- Michaeli S, Gröhn H, Gröhn O, et al. , 2005. Exchange-influenced T2 ρ contrast in human brain images measured with adiabatic radio frequency pulses. *Magn. Reson. Med. Off. J. Int. Soc. Magn. Reson. Med* 53, 823–829.
- Michaeli S, Oez G, Sorce DJ, et al. , 2007. Assessment of brain iron and neuronal integrity in patients with Parkinson’s disease using novel MRI contrasts. *Mov. Disord. Off. J. Mov. Disord. Soc* 22, 334–340.
- Michaeli S, Burns TC, Kudishevich E, et al. , 2009. Detection of neuronal loss using T1 ρ MRI assessment of 1H₂O spin dynamics in the aphakia mouse. *J. Neurosci. Methods* 177, 160–167. [PubMed: 19027791]
- Mitsumori F, Watanabe H, Takaya N, 2009. Estimation of brain iron concentration in vivo using a linear relationship between regional iron and apparent transverse relaxation rate of the tissue water at 4.7 T. *Magn. Reson. Med* 62, 1326–1330. [PubMed: 19780172]
- Mouches P, Forkert ND, 2019. A statistical atlas of cerebral arteries generated using multi-center MRA datasets from healthy subjects. *Sci. Data* 6, 1–8. [PubMed: 30647409]
- Østergaard L, Engedal TS, Aamand R, et al. , 2014. Capillary transit time heterogeneity and flow-metabolism coupling after traumatic brain injury. *J. Cereb. Blood Flow Metab. Off. J. Int. Soc. Cereb. Blood Flow Metab* 34, 1585–1598.
- Palombo M, Ianus A, Guerreri M, et al. , 2020. SANDI: a compartment-based model for non-invasive apparent soma and neurite imaging by diffusion MRI. *Neuroimage* 215, 116835. [PubMed: 32289460]
- Peters A, 2002. The effects of normal aging on myelin and nerve fibers: a review. *J. Neurocytol* 31, 581–593. [PubMed: 14501200]
- Reisberg D, 2013. *The Oxford Handbook of Cognitive Psychology*. Oxford University Press.
- Satzer D, DiBartolomeo C, Ritchie MM, et al. , 2015. Assessment of dysmyelination with RAFFn MRI: application to murine MPS I. *PLoS One* 10, e0116788. [PubMed: 25680196]
- Schmid F, Barrett MJ, Jenny P, et al. , 2019. Vascular density and distribution in neocortex. *Neuroimage* 197, 792–805. [PubMed: 28669910]
- Selvanayaki V, Sasikala K, 2020. Watershed stroke. *Asian J. Nurs. Educ. Res* 10, 483–486.
- Smith SM, Beckmann CF, Andersson J, et al. , 2013. Resting-state fMRI in the human connectome project. *Neuroimage* 80, 144–168. [PubMed: 23702415]
- Stüber C, Morawski M, Schäfer A, et al. , 2014. Myelin and iron concentration in the human brain: a quantitative study of MRI contrast. *Neuroimage* 93, 95–106. [PubMed: 24607447]
- Tariq M, Schneider T, Alexander DC, et al. , 2016. Bingham–NODDI: mapping anisotropic orientation dispersion of neurites using diffusion MRI. *Neuroimage* 133, 207–223. [PubMed: 26826512]
- Tournier JD, Mori S, Leemans A, 2011. Diffusion tensor imaging and beyond. *Magn. Reson. Med* 65, 1532. [PubMed: 21469191]
- Tuite PJ, Mangia S, Tyan AE, et al. , 2012. Magnetization transfer and adiabatic R1 ρ MRI in the brainstem of Parkinson’s disease. *Parkinsonism Relat. Disord* 18, 623–625. [PubMed: 22265140]
- Uddin MN, Figley TD, Marrie RA, et al. , 2018. Can T1w/T2w ratio be used as a myelin-specific measure in subcortical structures? Comparisons between FSE-based T1w/T2w ratios, GRASE-based T1w/T2w ratios and multi-echo GRASE-based myelin water fractions. *NMR Biomed.* 31, e3868.
- Venkat P, Chopp M, Chen J, 2016. New insights into coupling and uncoupling of cerebral blood flow and metabolism in the brain. *Croat. Med. J* 57, 223–228. [PubMed: 27374823]

- Zang YF, He Y, Zhu CZ, et al. , 2007. Altered baseline brain activity in children with ADHD revealed by resting-state functional MRI. *Brain Dev.* 29, 83–91. [PubMed: 16919409]
- Zuo XN, Ehmke R, Mennes M, et al. , 2012. Network centrality in the human functional connectome. *Cereb. Cortex* 22, 1862–1875. [PubMed: 21968567]

Author Manuscript

Author Manuscript

Author Manuscript

Author Manuscript

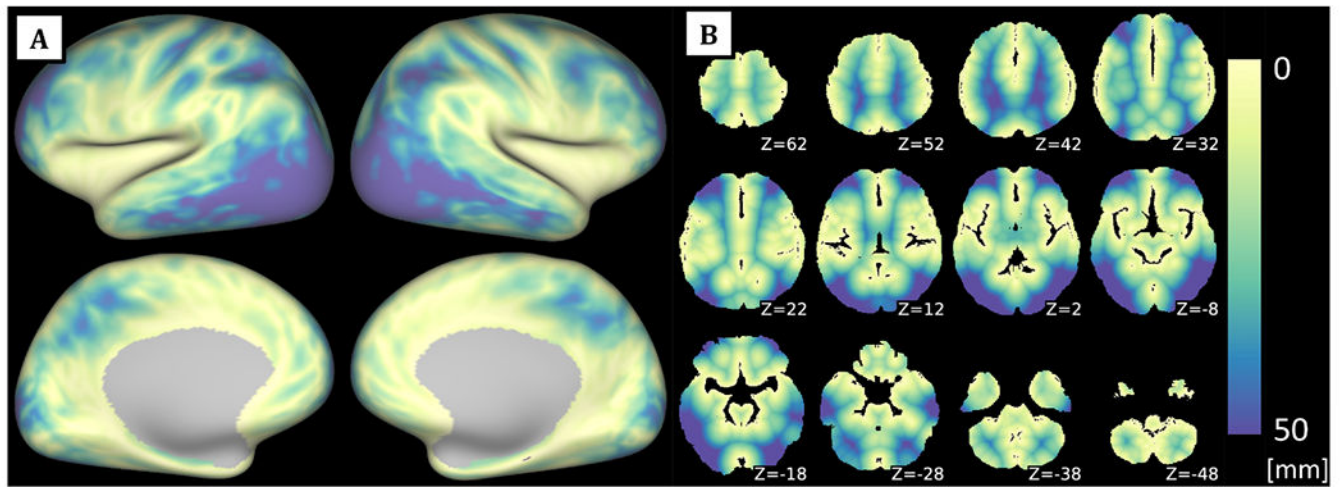


Fig. 1. Atlas of Euclidean distances to the nearest artery reconstructed on the surface (A) and in Montreal Neurological Institute (MNI) 3D space (B) based on the Statistical Atlas of Cerebral Arteries. White colour denotes areas relatively closer to the nearest artery, blue colour relatively more distant (see the colour scale at the right). Z values denote the level in z-axis (in mm) in the MNI space.

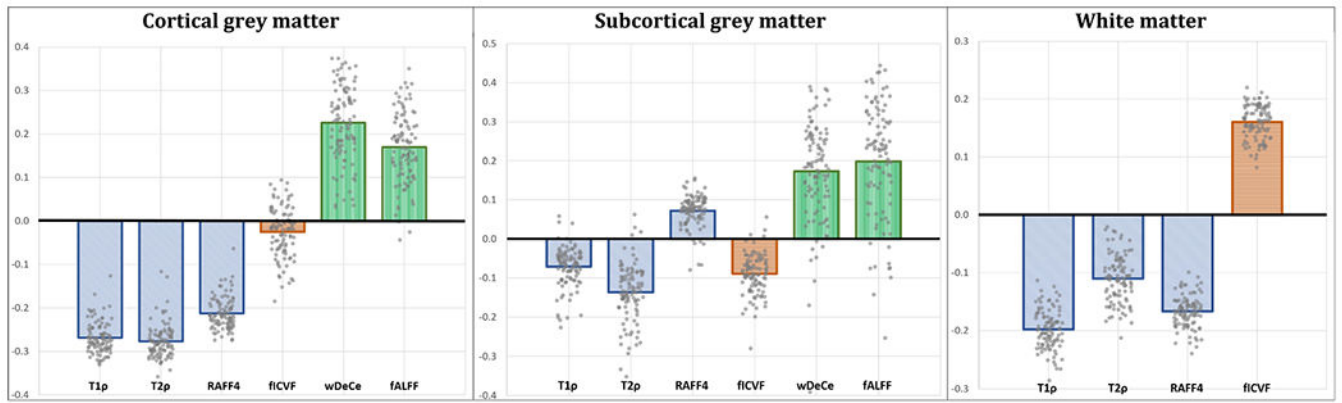


Fig. 2.

Average (bars) and individual (points) correlation coefficients of arterial distance and relevant quantitative MRI metric. Abbreviations: RAFF4 – relaxation along a fictitious field in the rotating frame of rank 4, fICVF – intracellular volume fraction; wDeCe – weighted Degree Centrality; fALFF – fractional amplitude of low-frequency fluctuations.

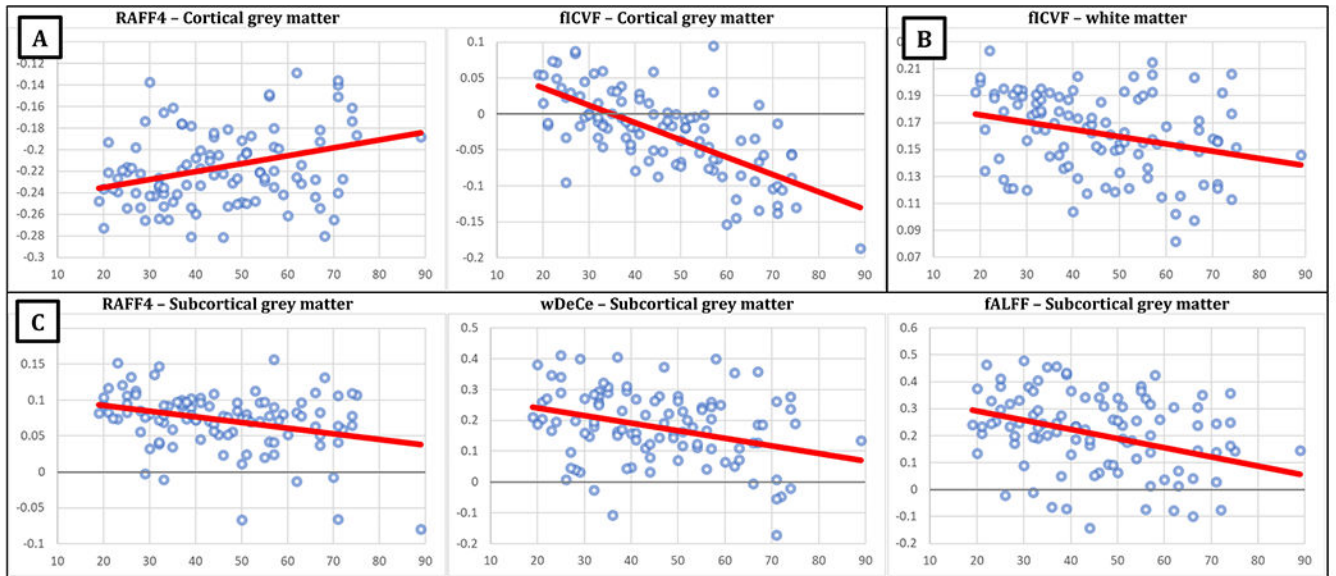


Fig. 3.

Scatterplots of the Spearman's rank correlation coefficients of arterial distance and relevant quantitative MRI metric (axis y) and age (axis x), with overlaid linear trendlines in red. Only statistically significant associations are shown: A –cortical grey matter; B – white matter; C – subcortical grey matter. For better visibility, zero y-level highlighted in scatterplots where the range of displayed values covered the value 0 on the y axis. Abbreviations: RAFF4 – relaxation along a fictitious field in the rotating frame of rank 4, fICVF – intracellular volume fraction; wDeCe – weighted Degree Centrality; fALFF – fractional amplitude of low-frequency fluctuations.

Table 1

Basic demographic information, body mass indices and daily activity levels for the full group and then divided into low/moderate/high activity based on IPAQ-SF guidelines. The values stated in the format median (range). Abbreviations: F – female, M – male, BMI – body mass index, IPAQ-SF - International Physical Activity Questionnaire, the short – self-administered version, MET – metabolic equivalent of task, min – minute.

	All group	Low activity	Moderate activity	High activity
Number of subjects	102	9	32	61
Age [years]	44 (19–89)	49 (21–89)	38.5 (19–71)	46 (20–75)
Sex [F/M]	53/49	4/5	17/15	32/29
BMI [kg/m ²]	24.9 (17.0–37.6)	24.9 (19.5–31.2)	25.6 (18.8–37.6)	24.2 (17–36.1)
IPAQ-SF [MET-min per day]	554 (0–3192)	14 (0–113)	286 (50–1166)	705 (285–3192)

Table 2

Average correlations between arterial distance and relevant quantitative MRI metrics and the effect of age on them, over three main regions of interest – cortical grey matter, subcortical grey matter, and white matter. Averages and standard deviations of subject-specific Spearman's rank correlation coefficients between MRI metrics and arterial distance are provided, followed by the T values, p values and Cohen's d (effect size) of the relevant one-sample *t*-test. The further columns provide the Pearson's correlation coefficient and its FDR corrected p-values for the analysis of age effect. Bold type and an asterisk marks statistically significant age effect. Abbreviations: AD – arterial distance; qMRI – quantitative magnetic resonance imaging metric; SD – standard deviation; RAFF4 – relaxation along a fictitious field in the rotating frame of rank 4, fICVF – intracellular volume fraction, wDeCe – weighted Degree Centrality; fALFF – fractional amplitude of low-frequency fluctuations, FDR – False discovery rate.

		Average [SD] of AD-qMRI correlations				Effect of age		
		T value	Cohen's d	FDR cor. p-value	Pearson's r	FDR cor. p-value		
Cortical grey matter	T1rho	-0.269 [0.036]	7.5	10 ⁻⁸⁸	0.138	0.333		
	T2rho	-0.277 [0.038]	7.3	10 ⁻⁸⁷	0.084	0.532		
	RAFF	-0.212 [0.036]	5.9	10 ⁻⁷⁸	0.315	0.006*		
	fICVF	-0.025 [0.057]	4.5	10 ⁻⁵	-0.683	10^{-14*}		
	wDeCe	0.226 [0.088]	25.1	10 ⁻⁴⁵	0.021	0.831		
	fALFF	0.17 [0.08]	21.0	10 ⁻³⁸	-0.153	0.288		
Subcortical grey matter	T1rho	-0.071 [0.051]	1.4	10 ⁻²⁵	-0.067	0.581		
	T2rho	-0.137 [0.073]	1.9	10 ⁻³⁴	0.091	0.531		
	RAFF	0.072 [0.041]	17.6	10 ⁻³²	-0.309	0.006*		
	fICVF	-0.089 [0.05]	-17.6	10 ⁻³²	-0.104	0.481		
	wDeCe	0.173 [0.126]	13.6	10 ⁻²⁴	-0.306	0.006*		
	fALFF	0.198 [0.155]	12.7	10 ⁻²²	-0.338	0.004*		
White matter	T1rho	-0.198 [0.034]	5.9	10 ⁻⁷⁸	-0.113	0.460		
	T2rho	-0.111 [0.041]	2.7	10 ⁻⁴⁷	-0.066	0.581		
	RAFF	-0.167 [0.027]	6.2	10 ⁻⁸⁰	0.027	0.831		
	fICVF	0.16 [0.029]	5.5	10 ⁻⁷⁶	-0.290	0.008*		